Title
Studies of energetic ion confinement during fishbone events in PDX

Journal
Nuclear Fusion, 25(8)

ISSN
0029-5515

Authors
Strachan, JD
Grek, B
Heidbrink, W
et al.

Publication Date
1985-08-01

DOI
10.1088/0029-5515/25/8/001

STUDIES OF ENERGETIC ION CONFINEMENT DURING FISHBONE EVENTS IN PDX

J.D. STRACHAN, B. GREK, W. HEIDBRINK, D. JOHNSON,
S.M. KAYE, H.W. KUGEL, B. Le BLANC, K. McGUIRE
Plasma Physics Laboratory,
Princeton University,
Princeton, New Jersey,
United States of America

ABSTRACT. The 2.5 MeV neutron emission from the beam-target d(d, n)^{3}He fusion reaction has been examined for all PDX deuterium plasmas which were heated by deuterium neutral beams. The magnitude of the emission was found to scale classically and to increase with $T_e^{3/2}$ as expected when electron drag is the primary energy degradation mechanism. The time evolution of the neutron emission through fishbone events was measured and used to determine the confinement properties of the energetic beam ions. Many of the experimental results are predicted by the Mode Particle Pumping Theory.

1. INTRODUCTION

High-beta operation on PDX exhibited a new instability called the fishbone instability [1, 2]. This instability was thought to be a large n = 1, m = 1 internal kink mode which also excited n = 1, m = 2, 3, 4 MHD modes because of the plasma outward shift at large poloidal beta. These MHD modes were correlated with a loss of energetic injected beam ions. In its most violent form, the fishbone instability could significantly reduce the flow of beam power to the plasma. The fishbone instability has been identified as one cause of beta saturation on PDX [1].

In this paper, the influence of the fishbone events on energetic ion confinement is inferred from neutron measurements on PDX. Previous PDX reports using the d(d, n)^{3}He reaction were limited to deuterium neutral-beam injection into hydrogen plasmas ($D^0 \rightarrow H^+$) [1, 2]. A major uncertainty in the interpretation of neutron data from these plasmas is that the relative concentration of hydrogen and deuterium in the plasma is not well known, making it difficult to evaluate the relative importance of beam/beam and beam/target reactions. Further, the relative importance of beam/beam reactions is higher during $D^0 \rightarrow H^+$ injection. In this paper, we examine all the available PDX data during $D^0 \rightarrow D^+$ injection. The major aim is to provide quantitative values of the energetic ion confinement time during fishbone events and to relate this confinement to other plasma parameters. The average and instantaneous confinement of the energetic beams ions can be described by the time evolution of the 2.5 MeV neutron emission from the beam/target d(d, n)^{3}He reactions. We find that the instantaneous energetic ion loss rate is proportional to the magnitude of the MHD oscillation ($\tilde{B}_\theta/B_\theta$), as is predicted by the Mode Particle Pumping Theory of White et al. [3]. Also, the average energetic ion confinement decreases when the product of toroidal beta and safety factor, βq, increases, which is in qualitative agreement with the expectations of pressure-driven kink models [1].

2. EXPERIMENT

2.1. Neutron diagnostics

The measurements reported here were made using the 2.5 MeV neutron emission from the d(d, n)^{3}He fusion reaction. These detector systems have been described previously [4] and their operation will only be briefly summarized here.

(a) The slow time evolution and the absolute magnitude of the 2.5 MeV neutron emission were detected by an array of moderated neutron detectors with 10 ms time resolution [4]. The absolute calibration was achieved using indium activation foils [5] placed on the PDX vessel. The accuracy of the measurement of the absolute emission level is probably about a factor of 1.5, including both systematic calibration uncertainties and counting statistics.

(b) High-frequency oscillations of the 2.5 MeV neutron emission were detected with an array of plastic NE102A and NE451 ZnS scintillators placed close to the vacuum vessel and connected by light pipes to photomultipliers [4]. The intrinsic detector frequency response is of the order of 1 MHz. In practice, the frequency response is limited by counting statistics to about 100 kHz resolution of a few per cent neutron oscillations at emission levels of $10^{14}\,s^{-1}$. In order to detect any possible contamination of the scintillator signal by hard X-rays, a NaI detector was used to measure hard X-rays produced by runaway electrons leaving the plasma. It was found that bursts of hard X-rays occurred during the H_α spikes of the edge relaxation phenomena [6] but not during fishbones (except when H_α spikes occurred simultaneously with the fishbones).

2.2. Interpretation

For the PDX plasmas with $D^0 \rightarrow D^+$ neutral-beam injection, the beam/target fusion reactions typically make up more than 75% of the total emission. The beam/beam reactions make up the remaining emission and the thermonuclear rates are unimportant (see Section 3.1). Insofar as the fusion emission can be described by beam-induced reactions, there are particularly simple relationships which relate the fusion emission to the confinement of energetic injected ions. For example, the rate of decay of the $d(d, n)^3He$ reaction during the fishbone yields the instantaneous confinement time, τ_B, of the most energetic of the injected ions.

For beam/target fusion reactions, the reaction rate, I_n, is approximately the product of the target deuterium density, n, the number of energetic ions, N, and the fusion reactivity σv evaluated at the energetic ion energy W [4].

$$I_n = nN(\sigma v)|_W \qquad (1)$$

The quantity N represents the cross-section-weighted energetic ion number

$$N \equiv \int\int f_b(r, \bar{v})\sigma\bar{v}\, d\bar{v}\, dr/(\sigma v)|_W$$

where f_b is the beam distribution function and the integral is over the plasma volume. The dominant contribution to N is from the portion of velocity space that is close to the full-energy component of the neutral-beam-injection energy and pitch angle.

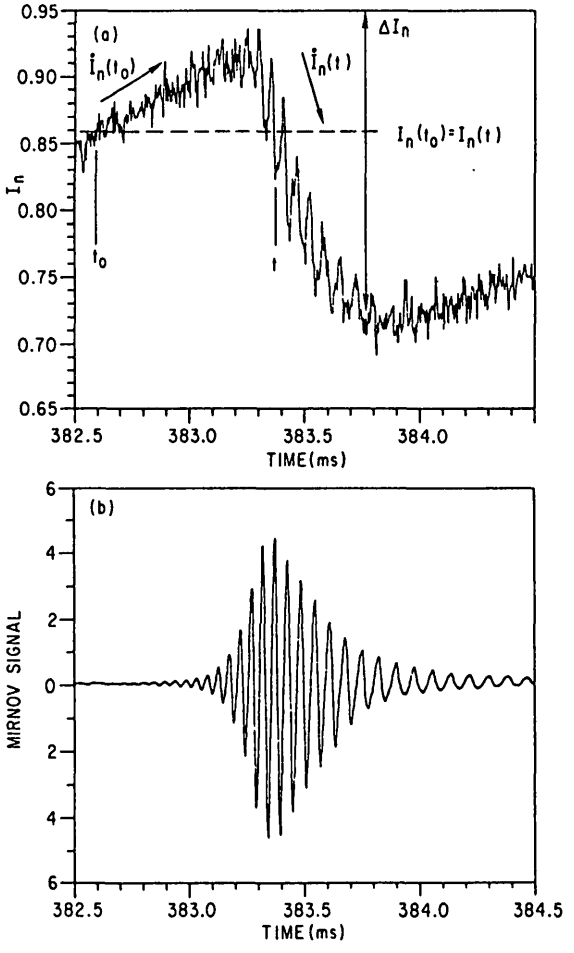

FIG.1. Time evolution of (a) the 2.5 MeV neutron emission and (b) the Mirnov signal through a fishbone instability having only a nominally 20 kHz oscillation.

The energetic ion population changes in time owing to the injection of additional beam ions at a source rate, S, and owing to the loss of energetic ions through thermalization or transport. It is convenient to consider separately the loss rate in the absence of fishbones, τ_n^{-1}, which is classically due to electron drag, and the losses during fishbones, which we characterize by a time-varying confinement time, $\tau_B(t)$. The rate of change of the energetic ion population, $\dot{N}$, is

$$\dot{N} = S - N/\tau_n - N/\tau_B(t) \qquad (2)$$

We can solve Eqs (1) and (2) to determine the evolution of the instantaneous confinement time $\tau_B(t)$ as

$$\tau_B(t) = \frac{I_n(t)}{\dot{I}_n(t_0) - \dot{I}_n(t)} \qquad (3)$$

where t_0 is a time before the onset of the fishbone instability such that $I_n(t_0) = I_n(t)$ and $\tau_B \gg \tau_n$, so that Eq. (2) becomes

$$\dot{N}(t_0) = S(t) - N(t)/\tau_n(t) \tag{4}$$

This means that using Eq. (3), one can determine the confinement time of the energetic (cross-section-weighted) beam ions by simply measuring the decay rate of the neutron emission during the fishbone, the neutron intensity, and the buildup rate of the neutron emission in the absence of the fishbone but at the same neutron intensity (see Fig.1). The only approximations are that the loss rate, τ_n^{-1}, the beam injection voltage, W, the source rate, S, and the deuterium target density, n, do not change between t_0 and t. Since the loss rate in the absence of fishbones is dominated by electron drag, these are all reasonable approximations.

The contribution of the beam/beam reactions to the total neutron emission is typically about 0.25 (see Section 3.1). If we consider a neutron emission composed of both beam/beam and beam/target emissions, then Eq. (1) becomes

$$I = I_{BT} + I_{BB} \tag{1a}$$

where $I_{BT} \propto N$ and approximately $I_{BB} \propto N^2$. The beam/beam reactions are only approximately proportional to N^2 since the relative velocity is higher and the slope of the cross-section is flatter so that lower-energy ions are relatively more important. If we define ϵ as the ratio of beam/beam reactions to beam/target reactions, $\epsilon = I_{BB}/I_{BT}$, then the derivation proceeds as before, with a slightly different derived energetic ion confinement time, τ_B^*

$$\tau_B^* \cong \tau_B\left(\frac{1+2\epsilon}{1+\epsilon}\right) \tag{3a}$$

where τ_B remains defined by Eq. (3). This means that if all reactions were beam/beam rather than beam/target, we would be underestimating the energetic-ion confinement time by a factor of two by using Eq. (3). For the PDX plasmas, ϵ is in the range of $0.2 \rightarrow 0.5$, at the highest beam power levels, indicating that the use of Eq. (3) can underestimate the energetic ion confinement time by at most 20–30%.

One can also define an average energetic ion confinement time $\langle\tau_B\rangle$ from the magnitude of the reaction drop at each fishbone, $\Delta I_n/I_n$ (Fig.1), and the period between fishbone events, P_{fb},

$$\langle\tau_B\rangle = \frac{P_{fb}}{\ln(1/(1 - \Delta I_n/I_n))} \tag{5}$$

This average confinement time is approximately the inverse of the energetic ion loss rate $\nu_{LOSS} \simeq 1/\langle\tau_B\rangle$ defined in Ref. [1]. It should be noted that τ_B and $\langle\tau_B\rangle$ are loss times of energetic ions from the energy range of W_B, the beam injection voltage (about 50 kV), to about 20 keV below W_B. More than 90% of the beam-induced fusion reactions come from this energy range because of the energy dependence of the fusion cross-section. The loss times τ_B and $\langle\tau_B\rangle$ may be either a particle loss from the plasma (to the walls), or an energy loss of ions confined in the plasma, or a combination of these two processes. In this paper, we tend to interpret the measured τ_B and $\langle\tau_B\rangle$ values as confinement times, since at least some energetic ions are lost from the entire plasma [8, 9]. However, we know that some ions gain considerable energy [1, 2] and that some ion cyclotron emission is also observed during the fishbones [9], so one might expect that many ions also lose considerable energy without necessarily being lost. Without quantitative measurements of fluxes of ions leaving the plasma, we can only note the above ambiguity in interpretation.

3. RESULTS

The data here represent all the available PDX neutron data during $D^0 \rightarrow D^+$ neutral beam operation ($B_\phi = 10 - 22$ kG, $I_\phi = 150 - 500$ kA, $P_B = 1 - 5$ MW, $a \simeq 0.4$ m, $R \simeq 1.4$ m).

3.1. Absolute neutron emission levels

Experimentally, the dominant scaling of the neutron emission, I_n, is

$$I_n \propto T_e^{1.63 \pm 0.07}\, P_B^{0.99 \pm 0.07}\, n_e^{0.19 \pm 0.05} \tag{6}$$

for constant $W_B = 45 \pm 2$ kV

where T_e is the central electron temperature, P_B is the applied beam power, n is the volume-averaged density, and W_B is the average beam voltage. A good fit is also attained (Fig.2) with

$$I \propto T_e^{3/2} P_B n^{1/2} W_B^2 \tag{7}$$

and the scaling holds over about two orders of magnitude in neutron emission.

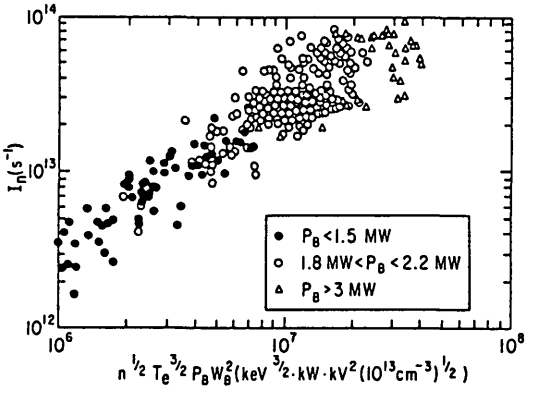

FIG.2. Neutron emission from PDX $D^0 \rightarrow D^+$ beam-heated plasmas scaled against $n_e^{1/2} T_e^{3/2} P_B W_B^2$. The beam power, P_B, is the power incident upon the plasma and is greater than that absorbed by the plasma.

If a confined beam ion slows down owing to electron drag, then, because of the strong dependence of the fusion reaction cross-section on energy, a typical beam ion has an appreciable probability of undergoing a fusion reaction for a time $\tau_n \simeq \tau_s/3$, where τ_n is the cross-section-weighted slowing-down time, and τ_s is the total slowing-down duration. If most of the injected beam ions are confined for a time long compared to the slowing-down time ($\tau_n \ll \langle\tau_B\rangle$), then the number of energetic beam ions in the hot plasma core is approximately [4]

$$N = \xi \dot{N}_B \tau_n \tag{8}$$

where ξ is the fraction of the injected beam ions captured in the central plasma regions, and $\dot{N}_B$ is the injection rate of the full-energy component of the beam ions. For electron drag, $\tau_n \propto T_e^{3/2}/n_e$, and for Z = 1 deuterium plasmas, one expects

$$I_n \propto \xi T_e^{3/2} P_B W_B^2 \tag{9}$$

Interestingly, the scaling of the neutron emission with the electron drag ($T_e^{3/2}$) is the single strongest scaling observed in the data (Fig.3). The observed density dependence (Eq.(6)) (Fig.4(a)) is possibly due to the penetration factor, ξ, which is a profile effect and is probably due to shine-through (reducing the absorbed power), and to some contribution from increased beam-ion charge-exchange losses at the lower densities. The density scaling can also be expressed as a neutral mean-free path, ℓ, scaling (Fig.4(b)). It is also likely that the ratio n_d/n_e increases with electron density (owing to a probable decrease in Z_{eff}), which might also contribute to the density dependence of Fig.4.

For a reduced set of the available PDX data, TRANSP runs [10] have also been made which predict the absolute neutron emission and which calculate the beam/target, beam/beam and thermonuclear neutron

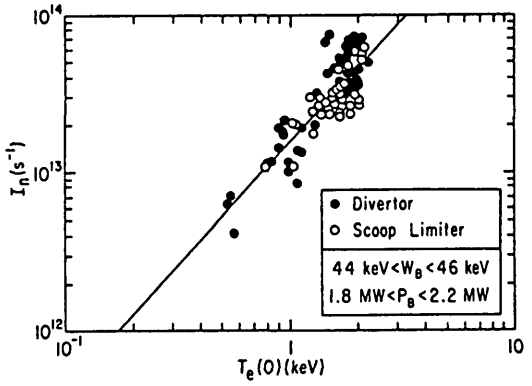

FIG.3. Neutron emission, I_n, from PDX $D^0 \rightarrow D^+$ beam-heated plasmas scaled against T_e at constant beam voltage and beam power. The dependence of $T_e^{3/2}$ is expected from classical electron drag. The solid line is a least-squares fit to the data.

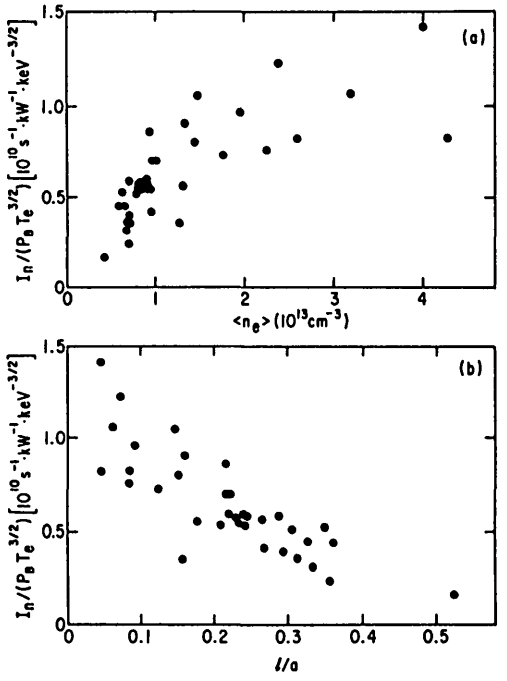

FIG.4. Neutron emission normalized to the electron temperature and beam power, $I_n/T_e^{3/2} P_B$, scaled with (a) the volume-averaged electron density, $\langle n_e\rangle$, and (b) the neutral mean-free path for a beam neutral ℓ/a. The data are restricted to constant beam voltage (42.5 keV < W_B < 46 kV).

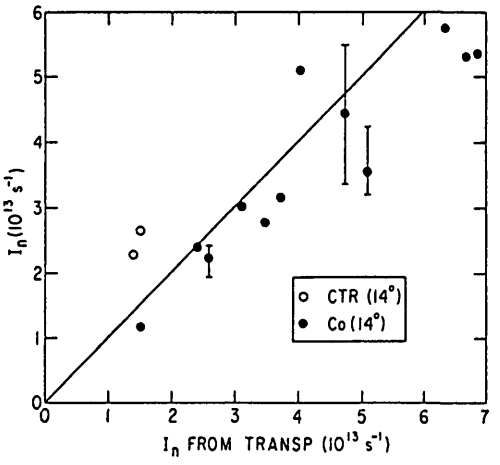

FIG.5. Experimental neutron emission compared to the TRANSP calculation of the beam/target plus beam/beam neutron emissions. The calculations use the experimental electron temperature and electron density profiles to calculate the classical deposition and slowing-down of the beam ions.

emission levels. The agreement between TRANSP and the experimental values (Fig.5) is good. TRANSP calculates that the beam/target reactions are about 75% of the total emission, with the remainder due to beam/beam reactions.

Essentially, the dominant empirical scaling of the neutron emission magnitude during $D^0 \rightarrow D^+$ corresponds to that expected for classical behaviour of beam/target fusion reactions. Apparently, the fishbone instability does not have a strong effect on the magnitude of the emission. This is expected if $\langle \tau_B \rangle \gg \tau_n$. However, at any one condition, there is still a large amount of scatter which could hide significant (about 50%) reductions in the neutron emission owing to the fishbone activity. It should be stressed again that we are discussing here the neutron emission values averaged over 10 ms periods and not the obvious 30% drops in the neutron emission observed for short times at the fishbone instability (e.g. Fig.1).

3.2. Instantaneous confinement times, τ_B

Energetic ion losses were observed with four types of events:

- the classic fishbone, with $\tilde{B}_\theta/B_\theta$ oscillating only in the range 10 – 20 kHz [2];
- a high-frequency event, with $\tilde{B}_\theta/B_\theta$ oscillating only in the range of 50 – 100 kHz;
- a double-frequency event, with $\tilde{B}_\theta/B_\theta$ oscillating both in the frequency range of 10–20 kHz and in a frequency range approximately 4–6 times higher;
- a sawtooth event, with $\tilde{B}_\theta/B_\theta$ oscillating in the range of 4–10 kHz.

  Sawtooth events with $\tilde{B}_\theta/B_\theta$ oscillating at higher frequencies (such as are mentioned in Ref. [2]) were not observed in the present data set.

Observations from each of these events will be described separately. In previous PDX publications, fishbones were considered to be only those events where an oscillation of 10–20 kHz is observed. Here we examined all events where the MHD signal is coupled to the plasma edge so that an oscillating signal is seen on the Mirnov coils [7]. Often, an energetic ion loss is inferred from the neutron emission for these events.

3.2.1. Single-frequency fishbones

If we examine the time evolution of a 20 kHz fishbone event (Fig.1) then we see that $\tilde{B}_\theta/B_\theta$ grows and falls exponentially (Fig.6). The neutron emission rises before the fishbone, while the magnetic oscillation at the edge of the plasma is small. The neutron signal begins decaying when the amplitude of the magnetic oscillation is near its maximum and, as it decays, it also exhibits the approximately 20 kHz internal fishbone oscillations with an amplitude $\tilde{I}_n/I_n \simeq 5\%$. During the fishbone event in Fig.1, the frequency of the magnetic oscillation decayed (Fig.6) from 22 kHz to approximately 11 kHz. The instantaneous confinement time of the energetic beam ions as determined from the decay rate of the neutron emission, using Eq. (3), falls exponentially (Fig.6) to about 1 ms and rises as the magnetic oscillation decreases. The influence of the 20 kHz neutron oscillation was ignored in deducing the neutron decay rate.

A strong correlation (Fig.7) exists between the instantaneous confinement time, τ_B (obtained using Eq.(3)) and the magnitude of the magnetic oscillation through the fishbone event of Fig.1

$$\tau_B \propto \left(\frac{\tilde{B}_\theta}{B_\theta}\right)^{-0.83 \pm 0.02} \tag{10}$$

A data base was formed of all available $D^0 \rightarrow D^+$ fishbone events and the peak $\tilde{B}_\theta/B_\theta$ was recorded as well as the magnetic oscillation frequency (at the peak neutron decay, before the neutron decay and after the neutron decay) and the neutron decay rate at the peak $\tilde{B}_\theta/B_\theta$. Figure 8 is a plot of the range of $\tilde{B}_\theta/B_\theta$ values

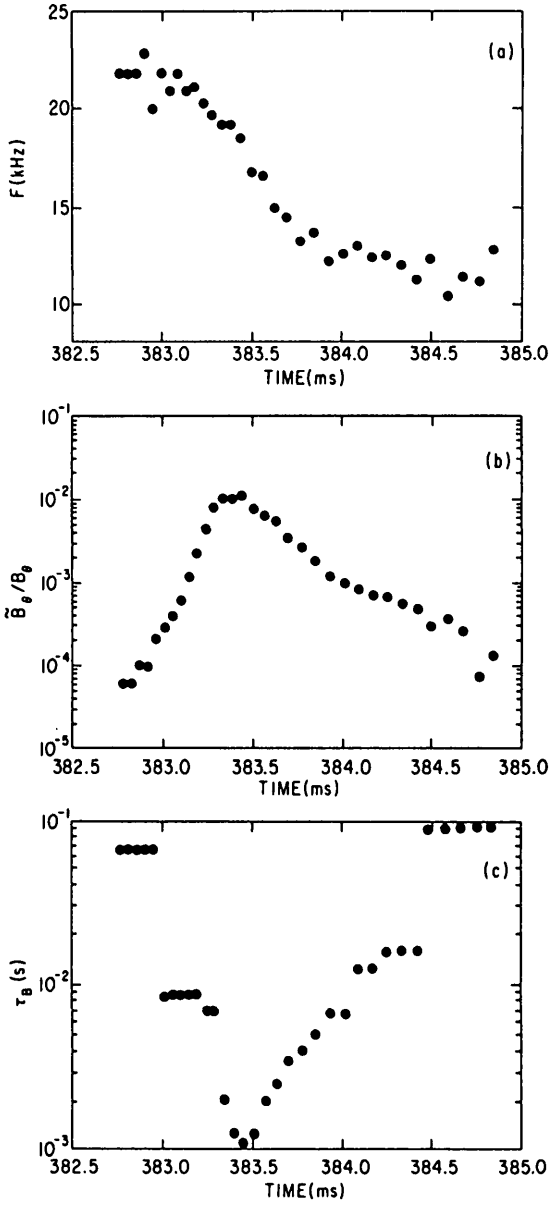

FIG.6. Time evolution of (a) the fishbone frequency, F; (b) the magnetic oscillation amplitude, $\tilde{B}_\theta/B_\theta$; and (c) the deduced instantaneous energetic ion confinement time, τ_B, for the fishbone in Fig.1.

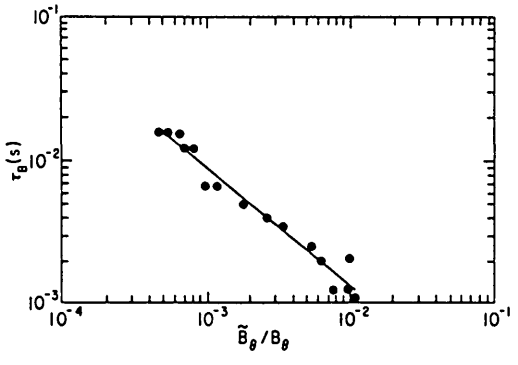

FIG.7. Scaling of the energetic ion confinement time, τ_B, with the magnetic oscillation amplitude, $\tilde{B}_\theta/B_\theta$, through the time-evolving fishbone event shown in Figs 1 and 6.

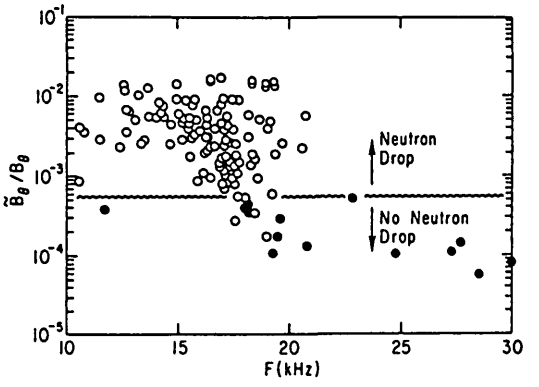

FIG.8. Peak magnetic perturbation amplitude, $\tilde{B}_\theta/B_\theta$, and fishbone frequency, F, at the peak amplitude for the events which make up the data base of 20 kHz fishbones. The open points had a measurable neutron drop ($\Delta I_n > 0.2\%$) while the solid points had $\Delta I_n \simeq 0$.

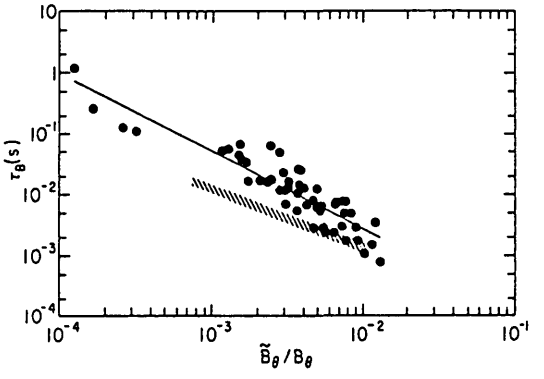

FIG.9. Minimum energetic ion confinement time, τ_B, as a function of the peak magnetic perturbation amplitude, $\tilde{B}_\theta/B_\theta$, for the single-frequency fishbone events. The hatched region represents the relation from Fig.7 which describes the evolution through a single fishbone.

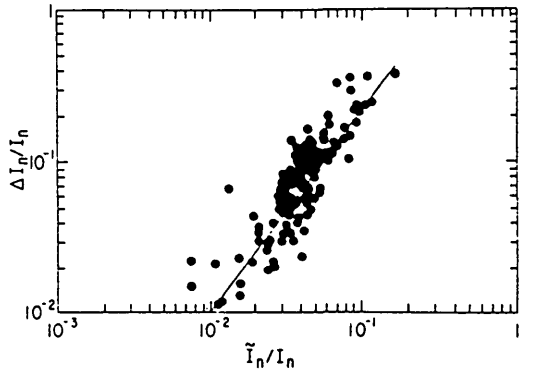

FIG.10. Fraction of energetic ions lost in the fishbone ($\Delta I_n/I_n$) as a function of the amplitude of the neutron oscillation at the fishbone frequency, $\tilde{I}_n/I_n$, for the single-frequency fishbone events. The line is a least-squares fit to the data.

and the fishbone frequency, F, at the peak neutron decay, for the single-frequency fishbone events. The solid points are events which did not have an observable (0.2%) drop in neutron emission associated with the magnetic oscillation. Evidently, there is an approximate threshold for observable loss of energetic ions of

$$\frac{\tilde{B}_\theta}{B_\theta} \gtrsim 10^{-3}$$

Examining all the events indicates that (Fig.9)

$$\tau_B \simeq 7.1 \times 10^{-6} \left(\frac{\tilde{B}_\theta}{B_\theta}\right)^{-1.36 \pm 0.07} \qquad (11)$$

Figure 9 differs from Fig.7 in that it represents the peak loss rates from many fishbone events, whereas Fig.7 represents the time evolution through a single event. Evidently, the losses at low $\tilde{B}_\theta/B_\theta$ values are more severe when they are associated with a larger event. The magnitude of the neutron drop ($\Delta I_n/I_n$), which is roughly the fraction of energetic beam ions lost during the fishbone event, is correlated with the minimum instantaneous ion confinement time, τ_B, indicating that the loss duration is about constant. Also, $\Delta I_n/I_n$ is correlated with the magnitude of the neutron oscillation at the fishbone frequency ($\tilde{I}_n/I_n$) (Fig.10).

The amount by which the frequency decreased during the fishbone (ΔF is the difference between the initial frequency before the neutron decay and the final frequency after the neutron decay has ended) depends on the initial frequency, F_i, and the eventual maximum size of the magnetic oscillation (Fig.11), scaling as

$$\Delta F \propto F_i^{2.42 \pm 0.2} \left(\frac{\tilde{B}_\theta}{B_\theta}\right)^{0.28 \pm 0.02} \qquad (12)$$

Since the $\tilde{B}_\theta/B_\theta$ values cover such a wide range of values, both F_i and $\tilde{B}_\theta/B_\theta$ are about equally important in the variation of ΔF in Eq. (12). Since there is a threshold in $\tilde{B}_\theta/B_\theta$ before there is a significant (measurable) loss of energetic ions (Fig.8), this means that there is a noticeable decrease in the frequency, even if there is no observable loss of energetic ions.

Scintillators placed poloidally and toroidally around the PDX plasma allowed the structure of the neutron oscillation at the internal fishbone frequency to be determined. These uncollimated detectors viewed only a small portion of the plasma immediately in front of the detector. The toroidal resolving angle (half-width of detector sensitivity) is about 45° [11]. The phase information we obtained is consistent with the interpretation that the neutron-emitting region inside the plasma has the same n = 1, m = 1 structure as exhibited by the central soft-X-ray emission, implying that the neutron fluctuation, $\tilde{I}_n$, arises primarily from the movement towards and away from the detector of the neutron-emitting region of the plasma. When the expression for neutron emission from a toroidal line source [6] is used, it is indicated that the magnitude of the neutron fluctuation, $\tilde{I}_n$, is linearly related to the radial extent of the plasma motion (Fig.12), with a 5% neutron oscillation corresponding to a plasma motion of about 7 cm. Measurement of the motion of the soft-X-ray hot spot indicates that the magnitude of the

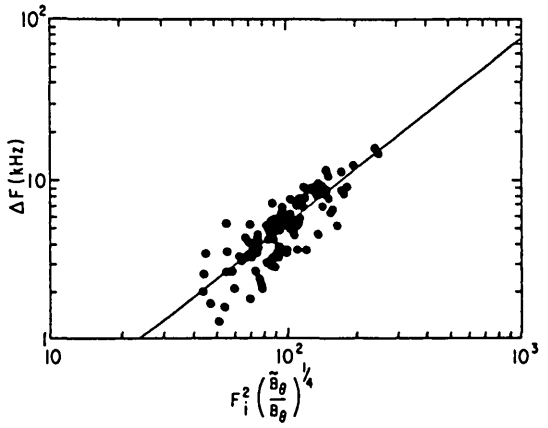

FIG.11. Best fit for the change in fishbone frequency (ΔF) (from the time before the neutrons began to decay until after they had finished decaying), showing a dependence of about $F_i^2(\tilde{B}_\theta/B_\theta)^{1/4}$ (F_i is the initial frequency).

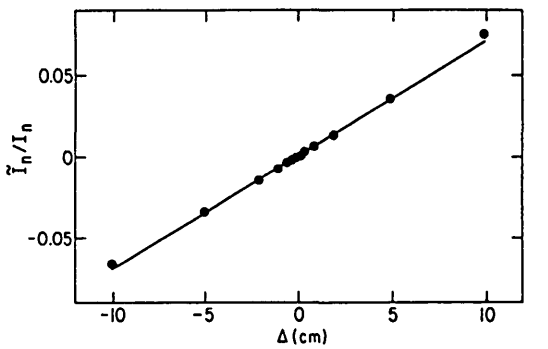

FIG.12. Calculated neutron fluctuation amplitude, $\tilde{I}_n/I_n$, versus in-out movement, Δ, of the neutron-emitting plasma. The points are calculated and the line is a fit to the points.

neutron fluctuation (Fig.13) can be explained by the magnitude of the central plasma in-out motion. The phase is such that the neutron fluctuation has a peak when the hot spot of the X-rays is shifted outwards (i.e. the hot region of the plasma is closest to the neutron detector). Evidently, the energetic ion population, the deuterium target density or both sets of ions form the same spatial structure as the MHD mode.

Some toroidal phase information was obtained by comparing the signal of two scintillators displaced toroidally by 180° but mounted at the same poloidal position (horizontal midplane). The signals were out of phase (Fig.14), indicating that the neutron signal had

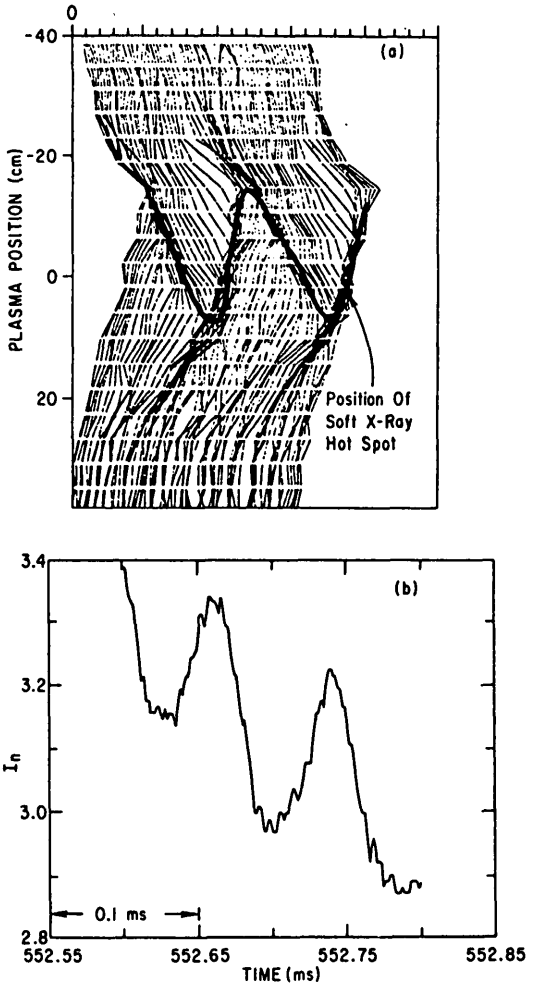

FIG.13. Phase correlation of (a) the movement of the plasma centre as determined by the central soft X-rays, and (b) neutron fluctuations at the fishbone frequency. The neutron signal peaks when the plasma centre has its maximum displacement towards the neutron detector. The soft-X-ray measurement is actually an up-down measurement. However, in this figure the phase has been changed in order to represent the in (negative) and out (positive) movement of the plasma in front of the neutron detector.

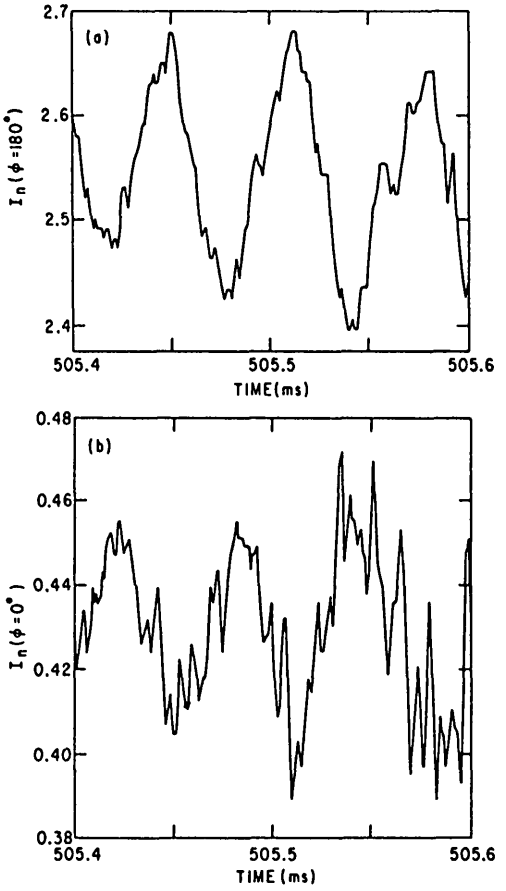

FIG.14. Toroidal phase information for two neutron detectors spaced 180° toroidally around PDX. Although the detectors are similar, their amplification was different, which accounts for the difference in signal levels.

an n = odd structure, consistent with the n = 1 structure of the MHD mode.

Some poloidal phase information was obtained by comparing the signal of two scintillators displaced poloidally by about 60° but at the same toroidal location. The detector signals had a phase lag consistent with motion in the ion diamagnetic direction, and the signals could be simulated in phase and magnitude by an m = 1 rotating structure of the neutron-emitting toroidal line source (Fig.15). This poloidal information rules out the possibility that the neutron fluctuation could be caused by an outwardly propagating beacon of energetic ions [3] moving in phase with the n = 1, m = 1 internal mode. Potentially, the beacon of the Mode Particle Pumping Theory could provide a neutron enhancement, since it allows for an energetic ion population to be in a location closer to the neutron detectors. Moreover, many of these ions have higher ion energies [8] and thus have larger fusion reactivities.

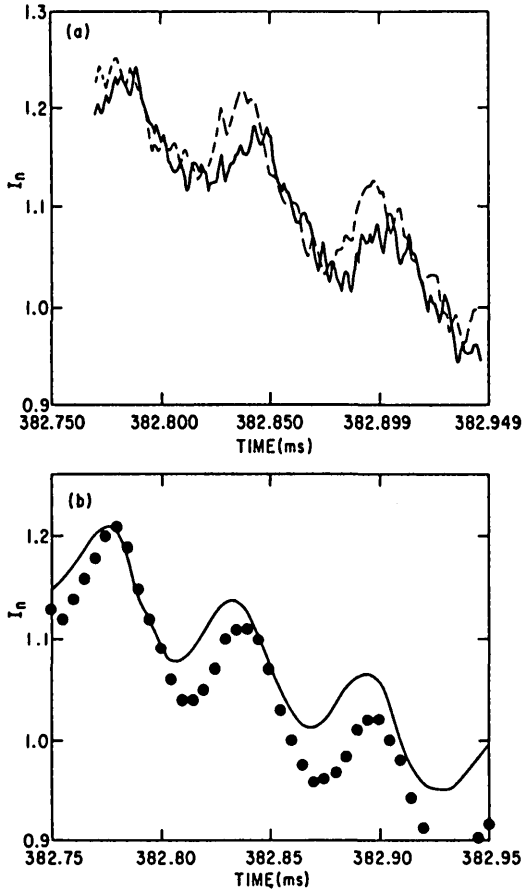

FIG.15. (a) Poloidal phase information from two neutron detectors at the same toroidal location but displaced poloidally by 54°.

(b) Calculated detector response to a decaying neutron signal superimposed on an m = 1 displacement of the neutron-emitting region of the plasma (rotating in the ion diamagnetic direction).

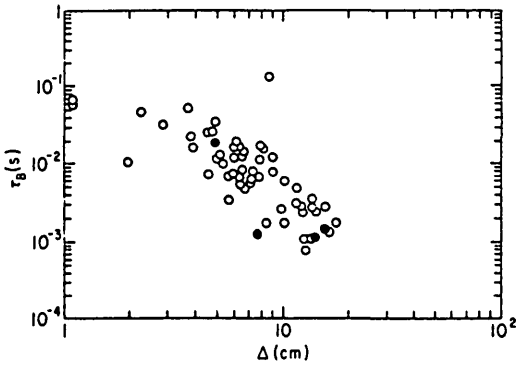

FIG.16. Relation between the energetic ion confinement time, τ_B, and the magnitude of the in-out plasma motion, Δ, which was determined from the neutron fluctuation amplitude, $\tilde{I}_n/I_n$ (Fig.12). The open points are the single-frequency fishbone events and the solid points are double-frequency fishbones with a large low-frequency perturbation.

However, the nature of the beacon loss process is that while it moves toroidally around the plasma with the fishbone magnetic perturbations, it always transports ions to the larger major radius side of the plasma and thus does not have the m = 1 structure. It should be emphasized that we are not ruling out the existence of such a beacon but only that the beacon did not cause the 20 kHz neutron fluctuation. The identification of the neutron fluctuation as a plasma in-out motion and the observed correlation of the magnitude of the neutron drop with the neutron fluctuation amplitude can also be interpreted as a correlation of the instantaneous ion confinement time with the magnitude, Δ, of the in-out motion (Fig.16). Approximately

$$\tau_B \propto (\Delta)^{-1.6 \pm 0.1} \qquad (13)$$

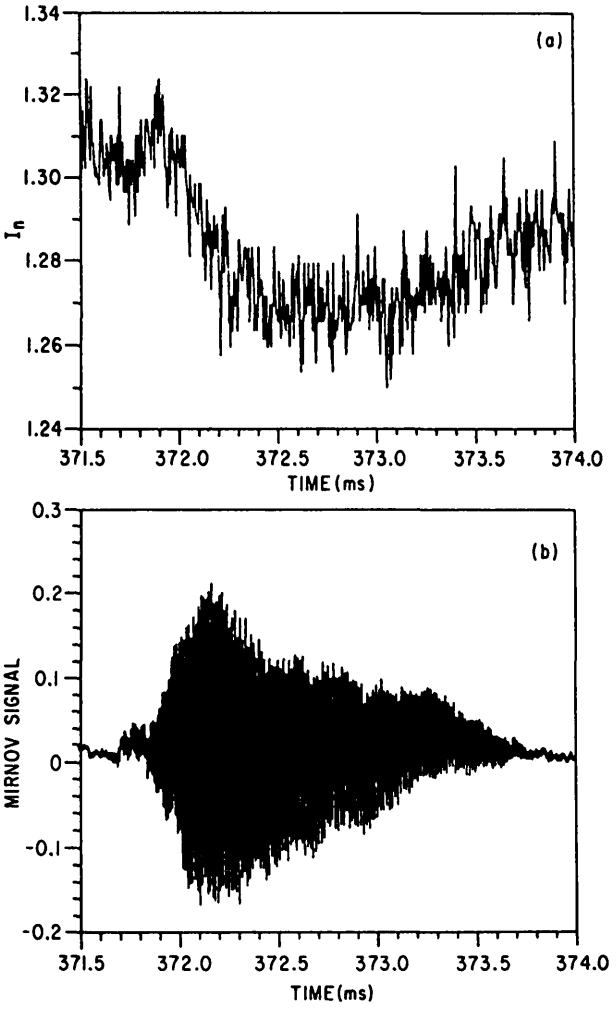

FIG.17. Time evolution of (a) the neutron emission and (b) the Mirnov signal for a high-frequency event.

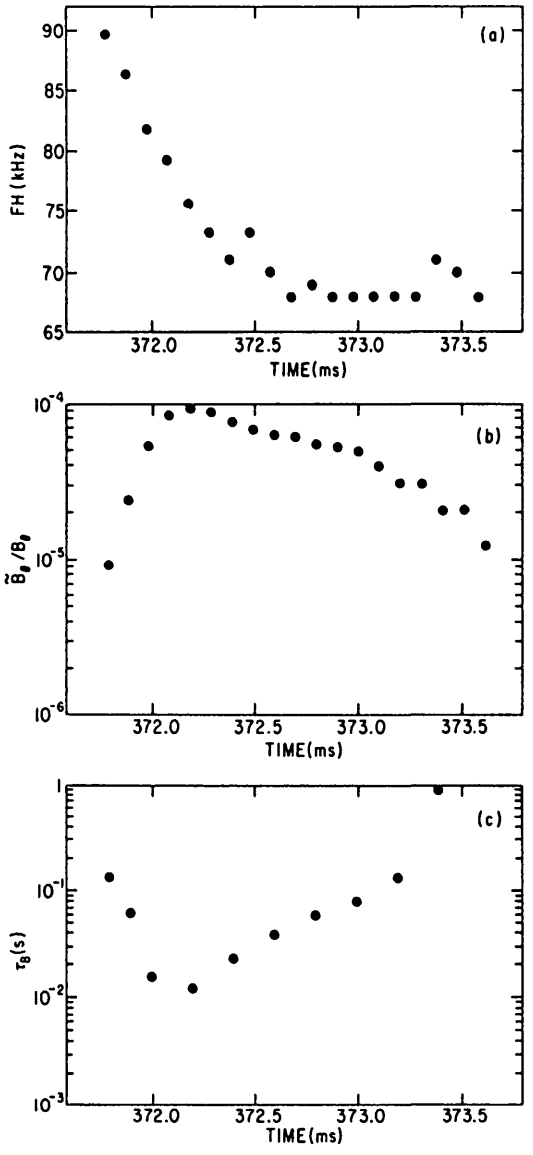

FIG.18. Time evolution of (a) the MHD oscillation frequency, FH, (b) the MHD magnetic perturbation amplitude, $\tilde{B}_\theta/B_\theta$, and (c) the energetic ion confinement time, τ_B, through the high-frequency event in Fig.17.

Alternatively, the same observation of the correlation of the magnitude of the neutron drop with the neutron fluctuation amplitude can be interpreted as a correlation with the ability of the energetic ions to redistribute into the spatial structure of the MHD mode.

3.2.2. High-frequency event

Occasionally, events occur with a single frequency which is usually higher than the normal fishbone frequency by roughly a factor of five. These events may not truly be related to the ~20 kHz fishbone events; however, they also experience a loss of energetic ions. Of themselves, these events were only a few per cent of all fishbone events and they did not have large drops in the neutron emission. However, quite often events occur with both high and low frequencies. In order to throw more light on the double-frequency events, we first examine the single high-frequency event.

The largest of these high-frequency events (Fig.17) has many similarities with the 20 kHz fishbones. The neutron emission drops as the magnetic oscillation reaches its peak and the frequency slows down considerably (Fig.18) as the energetic ions are lost (from 90 kHz to 65 kHz in this case). The magnetic perturbation at the Mirnov coil is much smaller ($\approx 10^{-4}$), which probably does not indicate that the higher-frequency oscillations are smaller inside the plasma but only that they attenuate more (owing to their higher m-number) between the plasma edge and the Mirnov coil.

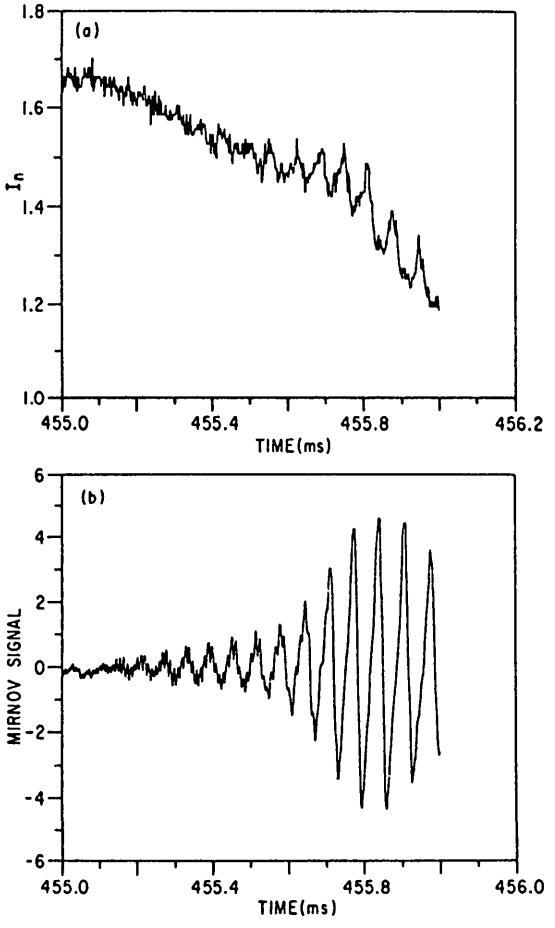

FIG.19. Time evolution of (a) the neutron emission, I_n, and (b) the Mirnov signal for a double-frequency fishbone.

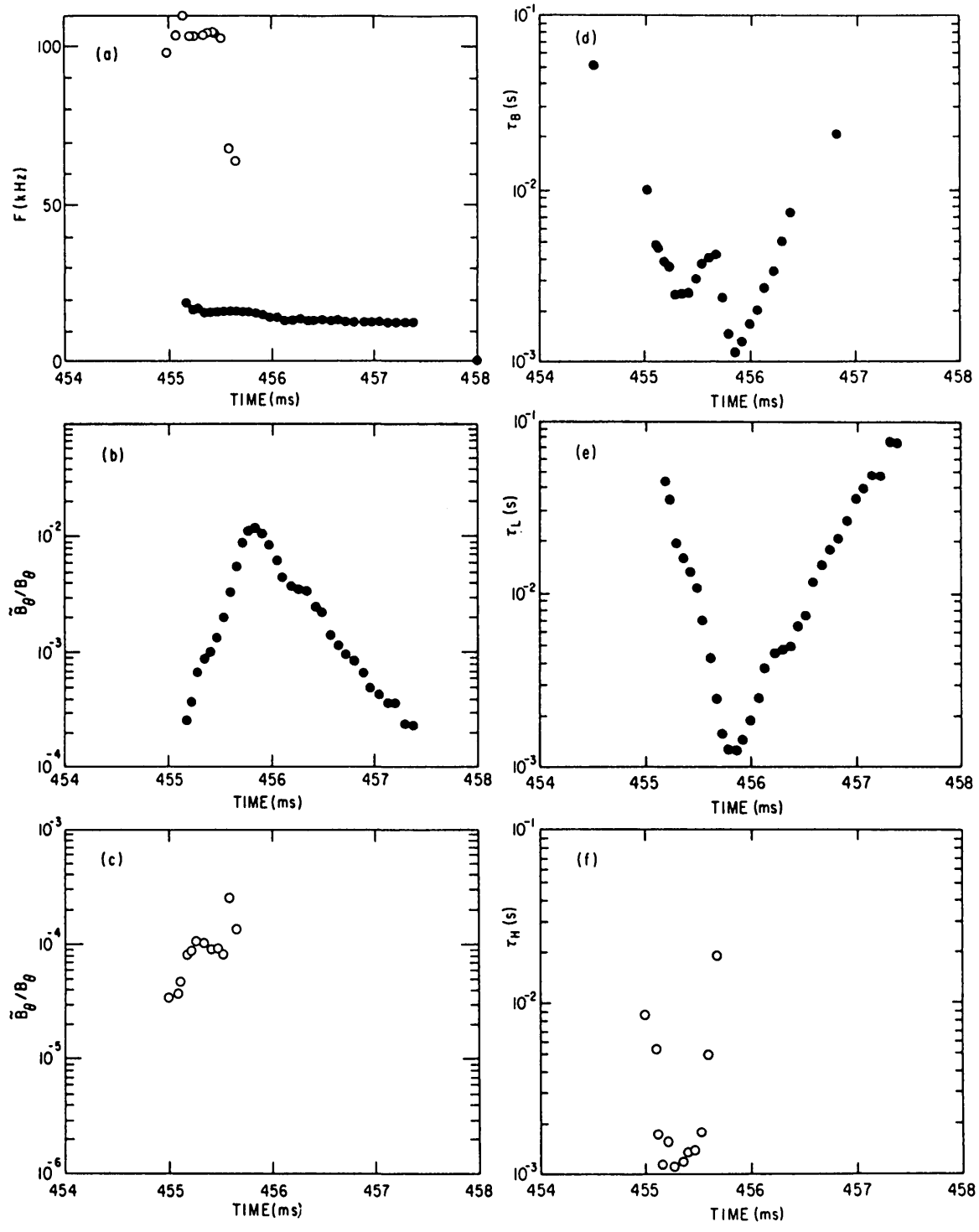

FIG.20. Time evolution of (a) the two frequencies; (b) the lower-frequency magnetic perturbation amplitude; (c) the higher-frequency magnetic perturbation amplitude; (d) the experimental energetic ion confinement time, τ_B; (e) the empirical confinement time, τ_L, from the single-frequency fishbones (Section 3.2.1); and (f) the empirical confinement time, τ_H, from the high-frequency events (Section 3.2.2) through the double-frequency fishbone in Fig.19.

As for the low-frequency events (Fig.6), the confinement time of the energetic beam ions also decays pronouncedly as the magnetic perturbation grows. A correlation of τ_B with $\tilde{B}_\theta/B_\theta$ (Fig.18) is again observed. The neutron counting statistics were too poor to see if any oscillations at the 5% level occurred during these events.

3.2.3. *Double-frequency fishbones*

Often, fishbone events have both ≈20 kHz magnetic oscillations and the 4 to 6 times higher frequency oscillation [2, 9]. The higher frequency will often precede the lower frequency (Fig.19 is a common example). Occasionally, however, the higher frequency will occur as a burst in the middle of the 20 kHz fishbone, or the 20 kHz oscillation will occur as a burst in the middle of an otherwise exclusively high-frequency event.

As occurs without the presence of the higher frequency, the approximately 20 kHz $\tilde{B}_\theta/B_\theta$ oscillation grows and decays nearly exponentially (Fig.20) while its frequency slows down. The time evolution of the energetic ion confinement time, τ_B, (Fig.20) has two minima, corresponding to the sequential peaking of the higher- and lower-frequency magnetic perturbations. The experimental confinement time is approximately a linear combination of the empirically scaled confinement times for the higher, τ_H, and lower, τ_L, frequency events

$$\frac{1}{\tau_B} = \frac{1}{\tau_H} + \frac{1}{\tau_L} \qquad (14)$$

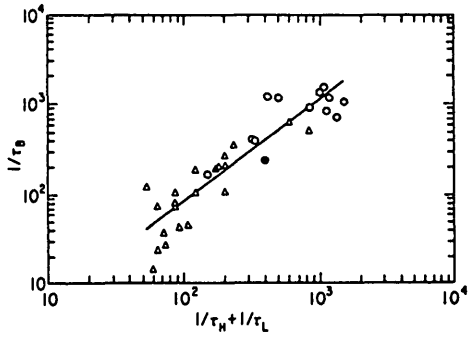

FIG.21. Minimum energetic ion confinement time, τ_B, for double-frequency fishbones as a linear combination of the sum of the empirically deduced high- and low-frequency events, τ_H and τ_L, using the measured magnetic perturbations at the time of the minimum energetic ion confinement. The solid point is the case without a low frequency (Fig.18), the open points are cases where the lower-frequency losses dominate, and the Δ points are cases where the higher-frequency losses dominate.

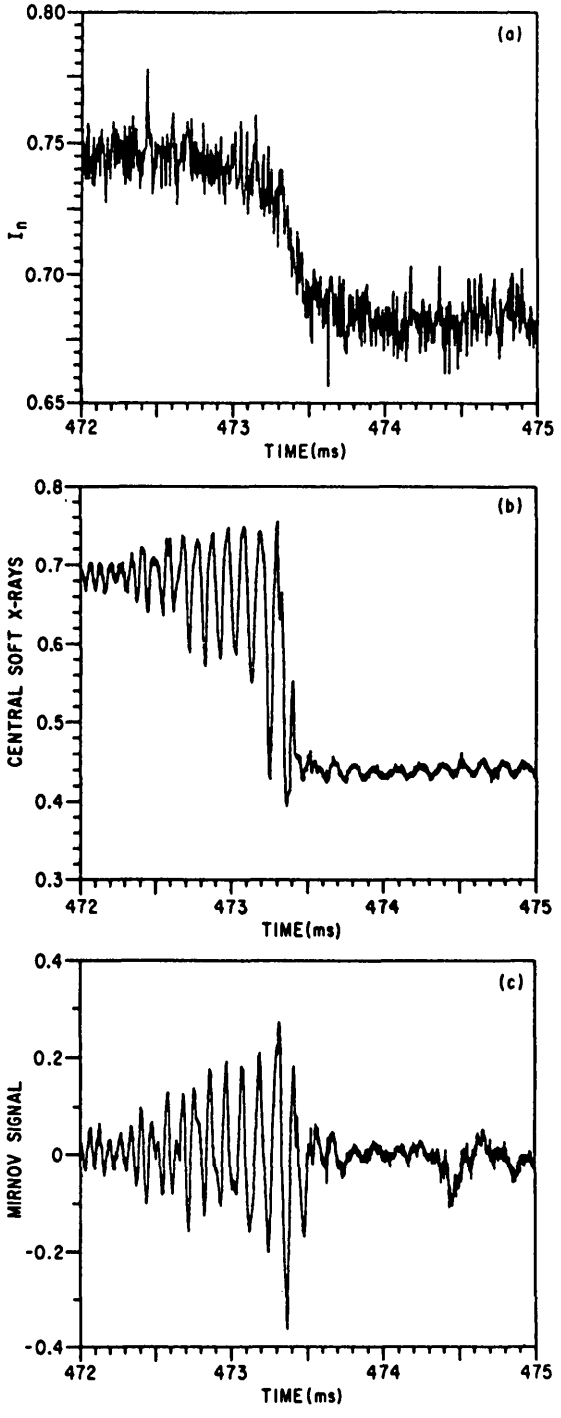

FIG.22. Time evolution of (a) the neutron emission, I_n; (b) the central soft X-rays; and (c) the Mirnov signal, for a PDX sawtooth event of the type with large energetic ion losses.

The peak energetic ion loss rate was examined for all the available $D^0 \rightarrow D^+$ cases where the two frequencies were present, and the loss rate was described by Eq. (14) (Fig.21).

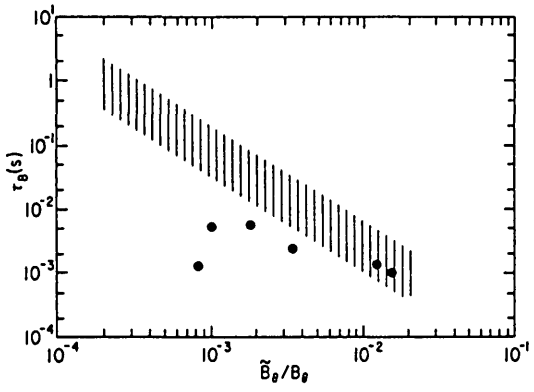

FIG.23. Energetic ion confinement time, τ_B, as a function of the external magnetic perturbation amplitude $\tilde{B}_\theta/B_\theta$ for the sawtooth events (e.g. Fig.22). The shaded region is the range of the data for the single-frequency fishbones (Fig.9).

3.2.4. *Sawtooth events*

A small number of sawtooth events occurred which also involved a large reduction in neutron emission ($\Delta I_n/I_n \approx 20$–$30\%$), indicating a loss of energetic ions. These events differ from more usual sawtooth events since the MHD frequency is higher (≈ 8 kHz) and the central n = 1, m = 1 MHD activity is coupled to the plasma edge and can be seen on the Mirnov coils (Fig.22). In sawtooth events involving only internal redistribution of energetic ions without significant loss to the walls, the neutron intensity drops by a small amount ($\Delta I_n/I_n \lesssim 3\%$) on a time-scale of the cross-section-weighted slowing-down ($\tau_n \approx 3$–5 ms) [4]. Larger drops on a faster time-scale can indicate losses of energetic ions at the sawtooth as well as some probable internal redistribution.

In fact, the particle loss for these events is severe and occurs during a single MHD oscillation period (Fig.22). Many of the sawtooth events (Fig.23) have larger losses of energetic ions than single-frequency fishbone events with the same measured values of $\tilde{B}_\theta/B_\theta$.

3.3. βq dependence

For PDX limiter discharges [1], the marginal stability condition for pressure-driven n = 1 internal kink modes

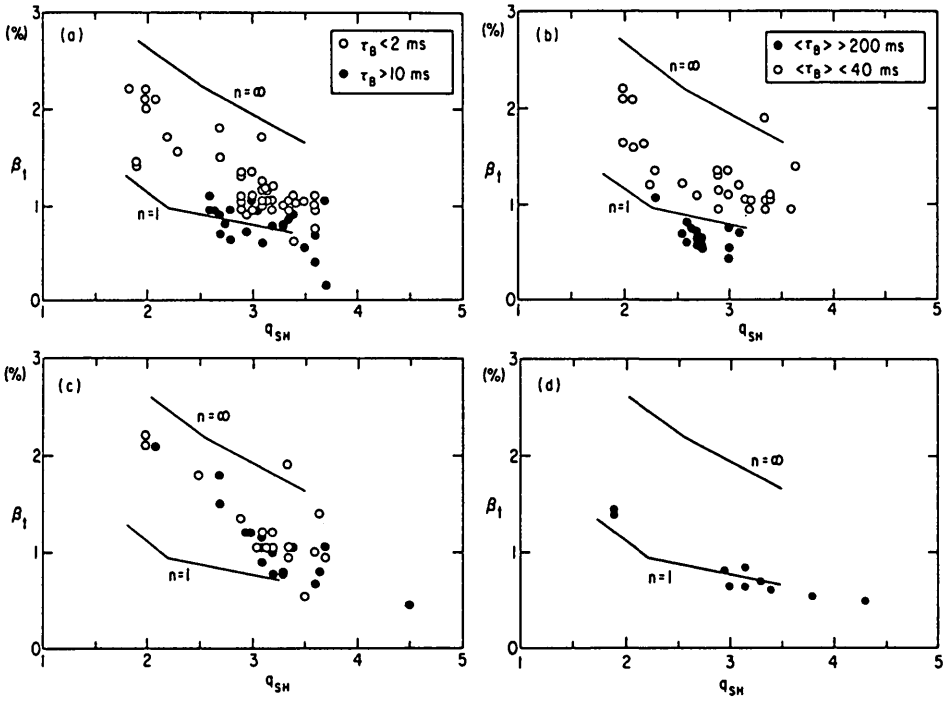

FIG.24. Location of plasmas having various types of fishbone events in βq space. (a) Single-frequency, 'classic' fishbone; (b) plasmas forming the $\langle\tau_B\rangle$ data base; (c) double-frequency events (open points are dominated by the lower frequency and solid points are dominated by the higher frequency); and (d) sawtooth events.

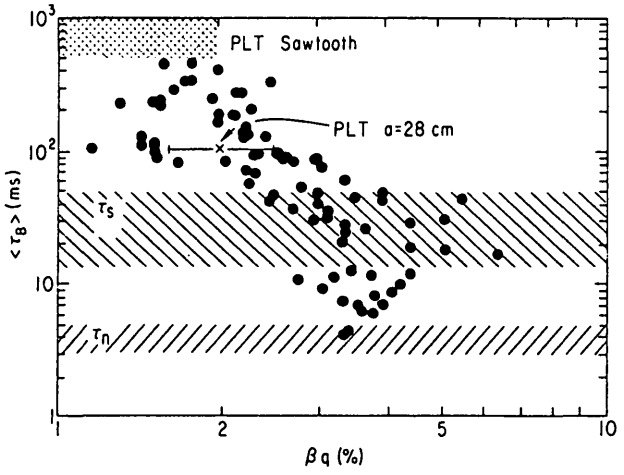

FIG.25. Scaling of average energetic ion confinement time, $\langle \tau_B \rangle$, with βq. The PLT sawtooth region is indicative of the calculated $\langle \tau_B \rangle$ for sawtooth events which probably feature only an internal energetic ion redistribution and not any energetic ion losses from the plasma [4]. The point for PLT, a = 28 cm, indicates a possible PLT fishbone event [12]; τ_s is a typical PDX slowing-down duration, and τ_n is the cross-section-weighted beam slowing-down time for typical PDX conditions.

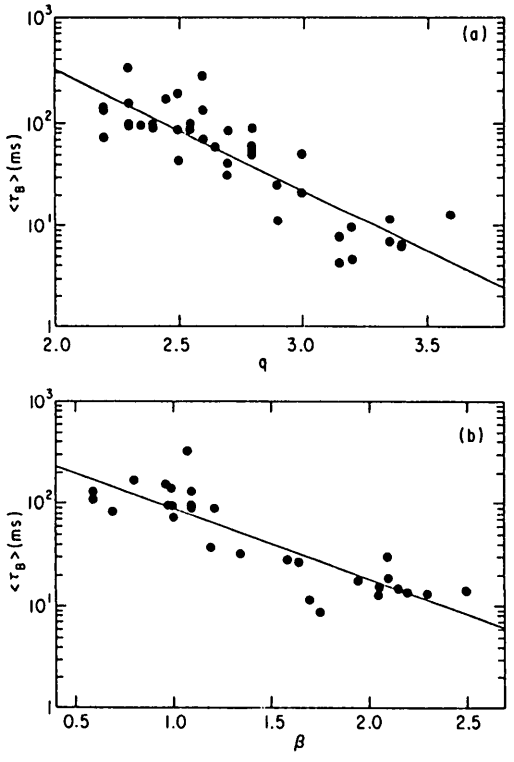

FIG.26. Scaling of average energetic ion confinement time, $\langle \tau_B \rangle$, for the data in Fig.25 when (a) q is varied but β is held constant ($0.8 < \beta < 1.2$), and (b) β is varied but q is held constant ($2 < q < 2.5$).

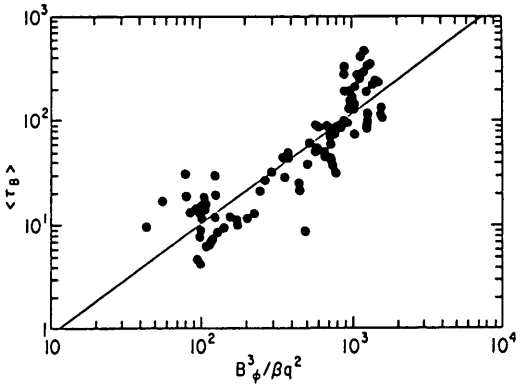

FIG.27. Scaling of average energetic ion confinement time, $\langle \tau_B \rangle$, with the parameter $B^3_\phi/\beta q^2$, which is an integer value form of the regression analysis using the data of Fig.25.

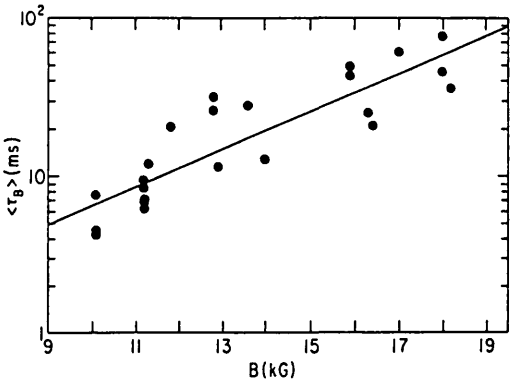

FIG.28. Dependence of average energetic ion confinement time, $\langle \tau_B \rangle$, on toroidal magnetic field at constant βq ($0.03 < \beta q < 0.04$).

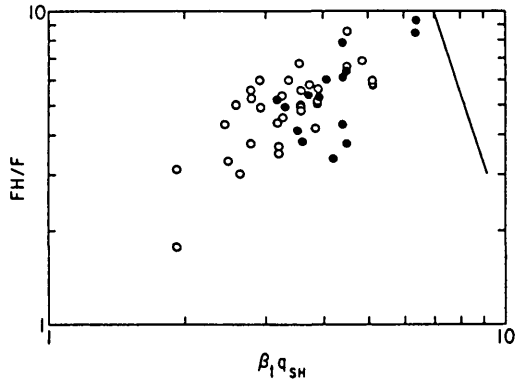

FIG.29. Ratio of the two frequencies, FH/F, in the double-frequency fishbones as a function of βq. The open points have the energetic ion losses dominated by the higher frequency, the solid points have the energetic ion losses dominated by the lower frequency. The line is the threshold condition quoted in Ref. [1].

is given by curves of constant $\beta q \simeq 0.021$, while the marginal stability condition for pressure-driven $n = \infty$ internal kink modes (ballooning modes) is given by $\beta q \simeq 0.05$; β is the toroidal beta and q is the Shafranov value [1]. These lines of marginal stability give only an indication of stability trends. Uncertainties in the actual q(r) and $\beta(r)$ profiles make the lines uncertain and the ballooning mode calculations are probably the more uncertain of the two. We find (Fig.24(b)) that the discharges with βq values above the n = 1 marginal stability curve do tend to have much larger average energetic ion losses. There exists a correlation of the average energetic ion confinement with βq of the form (Fig.25)

$$\langle \tau_B \rangle \propto (\beta q)^{-2.46 \pm 0.2} \quad (15)$$

The dependence of $\langle \tau_B \rangle$ on both β and q can be seen when the other parameter is held constant (Fig.26).

For the present data, the scaling of $\langle \tau_B \rangle$ with βq is equivalent to a scaling of $\langle \tau_B \rangle \propto (B_\phi / P_B)^2$. Doing a regression analysis (Fig.27) indicates that

$$\langle \tau_B \rangle \propto B_\phi^{3.1 \pm 0.4} \beta^{-1.1 \pm 0.2} q^{-2.5 \pm 0.4} \quad (16)$$

At constant βq ($0.03 < \beta q < 0.04$), $\langle \tau_B \rangle$ increases with B_ϕ (Fig.28), indicating that higher toroidal field experiments can have significantly reduced fishbone losses.

$$\langle \tau_B \rangle \propto B_\phi^{3.8 \pm 0.4} \quad (17)$$

Because of the particular data set available (since the current and the toroidal field are coupled), the scaling with toroidal field is equivalent to a scaling with plasma current, with approximately $\langle \tau_B \rangle \propto I_\phi^{0.8 \pm 0.2}$. Improved energetic ion confinement is expected in the Mode Particle Pumping Theory [3] for reduced banana width or increased plasma current, I_ϕ.

The amplitude of the fishbone event also depends on βq (Fig.24(a) – where from Fig.9 τ_B and $\tilde{B}_\theta / B_\theta$ are related). For the single-frequency event (Section 3.2.1), the minimum instantaneous energetic ion confinement time τ_B tends to be smaller when the plasma βq values are above the threshold for marginal stability [1] of the pressure-driven kink mode (Fig.24(a)). The high-frequency events (Section 3.2.2) and double-frequency events (Section 3.2.3) occurred in plasmas with parameters that were not noticeably different (Fig.24(c)) from those of plasmas in which the 20 kHz fishbone events occurred. No noticeable pattern distinguished the events where the higher frequency or the lower frequency dominated (Fig.24(c)). As was the case for the single-frequency events, there was a tendency for the most violent double-frequency events to occur above the n = 1 marginal stability line. The sawtooth events that involved losses of energetic ions (Section 3.2.4) occurred near the n = 1 marginal stability curve (Fig.24(d)). The ratios of the two frequencies in the double-frequency events tended to increase with βq (Fig.29). This coupling of the two frequencies to βq plus the apparent coupling of the strength of the individual fishbones to βq (Fig.25) probably indicate that the high- and low-frequency events have similar physical origins. The interpretation of the higher frequency as a higher n-mode would imply that the higher n-mode tended to occur at higher βq, while pressure-driven modes have the progression from n = 3 to $n = \infty$, occurring with lower βq [1]. Also apparent in Fig.29 is the tendency for the ≈20 kHz losses to dominate the events at the higher βq values.

4. DISCUSSION

4.1. Classical neutron emission

The dominant empirical scalings of the magnitude of the neutron emission during $D^0 \rightarrow D^+$ injection correspond to the scaling expected for classical behaviour of beam/target fusion reactions (Section 3.1). Apparently, for these PDX plasmas, the fishbone instability was not the dominant effect on the magnitude of the neutron emission. As described in Ref. [1], calculations of the gross energy confinement time indicate that fishbone losses do affect power deposition in the thermal plasma when the average energetic ion confinement time is reduced to about the beam ion slowing-down duration ($\tau_s \simeq 15 - 50$ ms for PDX conditions). These times become comparable for $\beta q \gtrsim 0.03$, a condition often achieved on PDX. The fishbone losses were not severe enough to reduce the average neutron emission rate seriously (i.e. by more than about 50%, or the measurement uncertainty), since this requires that the average confinement time $\langle \tau_B \rangle$ be less than the cross-section-weighted beam slowing-down duration τ_n (Section 2.2), and τ_n ($\tau_n \approx \tau_S/3$) was generally less than $\langle \tau_B \rangle$ (Fig.25).

4.2. Comparison with the 'Mode Particle Pumping' Theory

White et al. [3] describe an energetic ion loss process caused by magnetic field distortions of the types that occur during the fishbone events. This 'Mode Particle Pumping' Theory predicts a convective loss of energetic

ions due to $\vec{E} \times \vec{B}$ drifts associated with the MHD mode. According to this theory, the loss would be especially severe when the MHD frequency happens to equal the energetic ion precession frequency. The particles are predicted to be lost on the large major radius side of the plasma at one toroidal location which rotates around the device in phase with the MHD mode.

The minimum confinement time for the energetic ions can be written as

$$\tau \simeq \frac{a}{2\dot{r}} \tag{20}$$

where $\dot{r}$ is the average minor radial velocity of the most energetic ions given by Eq. (24) of Ref. [3]

$$\langle \dot{r} \rangle \simeq \frac{R \cos(\delta)\, m\, \alpha_{nm}\, \omega_p J_0(m\theta_b)}{r\left(1 - \frac{nq}{m}\right)} \tag{21}$$

where $\cos(\delta) \sim 1/4$ is the phase between the mode and the particle,

$m \simeq 3$

$1 - nq/m \simeq 1/2$

$J_0(m\theta_b) \simeq 1$ (θ_b is bounce angle)

$r \simeq a$

$\alpha_{nm} \propto (\tilde{B}_\theta/B_\theta)\, a^2/qR$

ω_p = precession frequency

being typical parameters for the illustrative case of Ref. [3], where the m = 3 mode (caused by the outshifted n = 1, m = 1 central perturbation) is causing most of the energetic ion loss. Thus

$$\tau_{min} \propto \frac{q}{\left(\frac{\tilde{B}_\theta}{B_\theta}\right) F} \tag{22}$$

and the constant of proportionality is obtained from Fig.4 of Ref. [3] which applies for a 0.5 ms MHD burst with $\tilde{B}_\theta/B_\theta$ of 1%, as measured at the Mirnov coils (also the value used in our experimental comparisons, e.g. Figs 6–8).

A comparison of the minimum loss time with the experimental values, either through the fishbone of Fig.1 (Fig.30) or through the peak loss rates (Fig.31), indicates good agreement. The principal dependence tested by the correlation is $\tau \propto \tilde{B}_\theta/B_\theta$. The factor-of-two-to-five displacement between theory and experiment is not significant since many simplifying

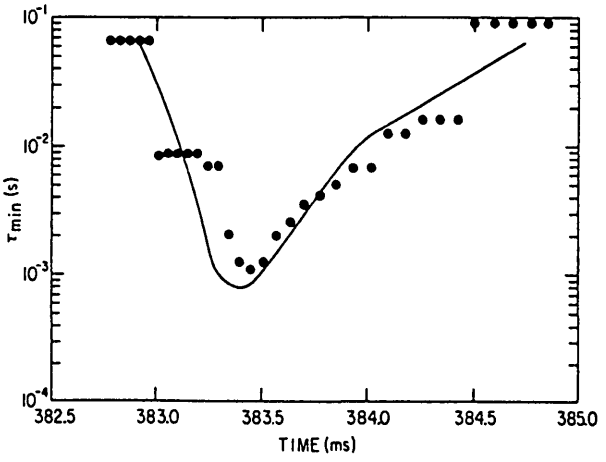

FIG.30. Time evolution of the theoretical minimum confinement time, τ_{min}, predicted by the Mode Particle Pumping Theory (line) for the fishbone event in Fig.1 (points).

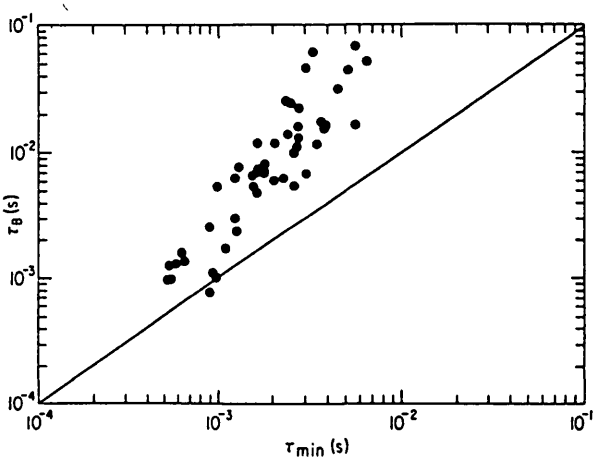

FIG.31. Comparison of the experimental energetic-ion confinement time, τ_B, with the minimum confinement time, τ_{min}, predicted by the Mode Particle Pumping Theory.

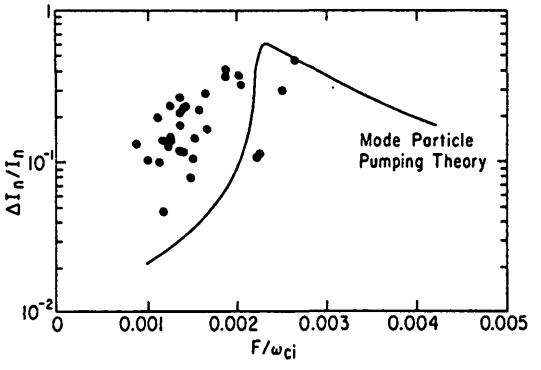

FIG.32. Percentage of beam ions lost for single-frequency fishbone events, with ($0.6\% < \tilde{B}_\theta/B_\theta < 1\%$), as a function of the fishbone frequency normalized to the ion cyclotron frequency [3]. The line is the prediction of the Mode Particle Pumping Theory for $\tilde{B}_\theta/B_\theta = 1\%$ (as measured at the Mirnov coil).

assumptions were made (above) in order to make the comparison, and also the calibration uncertainty of the Mirnov signal [7] alone could account for the difference.

Possibly of more significance is the comparison of the peak loss rates with the off-resonance 'Mode Particle Pumping' loss rates (Fig.4 of Ref. [3]). The data in Fig.32 indicate that the resonant condition might be broader than predicted in Ref. [3]. This is possible, since Ref. [3] considers a monoenergetic ion population with a fixed q(r) and a fixed cold plasma $\beta(r)$ profile. It should also be pointed out that we are taking the edge beam ion precession frequency including the finite-β correction, but not plasma rotation effects.

Reference [3] infers that the frequency change through the fishbone could mean that the part of velocity space which is lost is also changing, so that the resonant condition sweeps through the beam ions, ejecting ions of lower energy as the frequency slows down; this is probably not correct. Since the neutron cross-section changes roughly as $I_n \propto W_B^3$, a roughly cubic frequency dependence would be seen in the scaling of $\dot{I}$ (equivalently τ_B) or $\Delta I_n/I_n$; however, no such dependence was seen (for example, $\tau_B \propto F^{-0.24 \pm 0.8}$). Moreover, from Fig.22, a change in frequency is obtained even without a measurable loss of energetic ions.

4.3. Empirical confinement model

The number of energetic ions lost from the plasma during the fishbone ($\Delta I_n/I_n$) and the instantaneous energetic ion confinement time, τ_B, are both correlated with the neutron oscillation amplitude, $\tilde{I}_n/I_n$ (Fig.10)

$$\tau_B \propto \left(\frac{\tilde{I}_n}{I_n}\right)^{-2} \tag{23}$$

The neutron fluctuation amplitude is approximately linearly related to the magnitude of the in-out displacement, Δ, of the energetic ions by the internal n = 1, m = 1 MHD mode (Fig.12). Thus, τ_B is approximately (Fig.16)

$$\tau_B \propto \Delta^{-2} \tag{13}$$

The form of Eq.(13) suggests a modelling of the energetic ion losses by a diffusive process, where the diffusive step length is related to the MHD displacement of the energetic ions on axis, Δ, and the diffusion occurs at the magnitude of the internal fishbone frequency, F. Thus

$$D \simeq \left(\frac{\Delta}{2}\right)^2 F$$

$$\tau_D \simeq \frac{a^2}{D} \simeq \frac{4a^2}{\Delta^2 F} \propto \left(\frac{\tilde{B}_\theta}{B_\theta}\right)^{-1} F^{-1} \tag{24}$$

For the single-frequency fishbone events, the agreement between this model and the experiment can be made quite good over about two orders of magnitude in τ_B (Fig.33) by noting that a threshold of $\tilde{B}_\theta/B_\theta > 10^{-3}$ was required for observable fishbone losses (Fig.8). This threshold is equivalent to a threshold of Δ = 1 cm (or about the energetic ion gyroradius). The step size then becomes (Δ−1 cm), yielding

$$\tau_D \simeq \frac{a^2}{(\Delta-1)^2 F}$$

Of course, the scaling of τ_B with τ_D arises entirely from the two-orders-of-magnitude variation in $\tilde{B}_\theta/B_\theta$ in the data, and the factor-of-two variation of F plays no role.

Physically, this empirical model suggests that the energetic ions are being randomly transported in minor radius over distances of about the scalelength of the MHD perturbations, on a time-scale of about the MHD transit frequency of the machine, independent of any resonance of the energetic ions with the MHD wave. Such a thought process would then predict energetic ion losses for MHD bursts for different injection angles, as for the tangential injection on PLT [12].

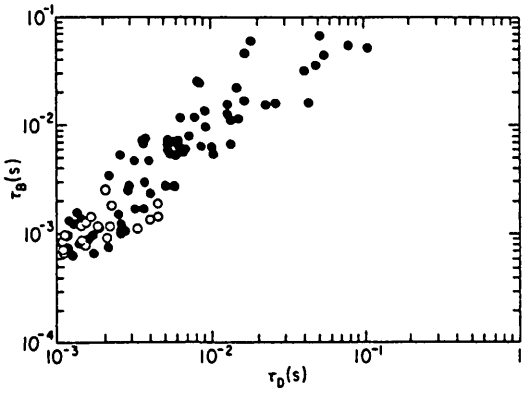

FIG.33. Energetic-ion confinement time, τ_B, compared with the simple diffusive loss model time, τ_D. The solid points are single-frequency events and the open circles are double-frequency events.

5. CONCLUSIONS

Quantitative measurements of the energetic ion confinement time during fishbone events on PDX were deduced from the beam/target neutron emission. The principal results were as follows:

(a) The average confinement time, $\langle\tau_B\rangle$, decreased when βq increased.
(b) The instantaneous confinement time, τ_B, was inversely related to the MHD perturbation amplitude, $\tilde{B}_\theta/B_\theta$.
(c) The energetic ion losses during sawtooth events and during high-frequency events are as large as the losses during 20 kHz fishbone events.
(d) Many features of the energetic ion losses observed here can be described by the Mode Particle Pumping Theory. The principal exception would seem to be that the resonance condition might be broader than described in the literature [3].

ACKNOWLEDGEMENTS

The authors thank K. Bol and the PDX operations group for their support of these experiments. Helpful discussions with P. Beiersdorfer, M. Bell, D. Buchenhauer, L. Chen, R. Goldston, G. Hay, R. Kaita and R. White are fully appreciated. The technical assistance of G. Estepp and F. Doughty in collecting the data and forming the large data bases was invaluable.

This work was supported by the United States Department of Energy, Contract No. DE-AC02-76-CHO-3073.

REFERENCES

[1] JOHNSON, D., BELL, M., BITTER, M., BOL, K., BRAU, K., et al., in Plasma Physics and Controlled Nuclear Fusion Research 1982 (Proc. 9th Int. Conf. Baltimore, 1982), Vol. 1, IAEA, Vienna (1983) 9.
[2] McGUIRE, K., GOLDSTON, R., BELL, M., BITTER, M., BOL, K., et al., Phys. Rev. Lett. **50** (1983) 891.
[3] WHITE, R.B., GOLDSTON, R.J., McGUIRE, K., BOOZER, A.H., MONTICELLO, D.A., PARK, W., Phys. Fluids **26** (1983) 2958.
[4] STRACHAN, J.D., COLESTOCK, P.L., DAVIS, S.L., EAMES, D., EFTHIMION, P.C., et al., Nucl. Fusion **21** (1981) 67.
[5] ZANKL, G., STRACHAN, J.D., LEWIS, R., PETTUS, W., SCHMOTZER, J., Nucl. Instrum. Methods **185** (1981) 321.
[6] FONCK, R.J., BEIERSDORFER, P., BELL, M., BOL, K., BOYD, D.A., et al., in Heating in Toroidal Plasmas (Proc. 4th Joint Varenna-Grenoble Int. Symp. Rome, 1984), Vol. 1, Int. School of Plasma Physics, Perugia (1984) 37. WAGNER, F., BECHER, G., BEHRINGER, K., Phys. Rev. Lett. **49** (1982) 1408.
[7] HAMMETT, G., McGUIRE, K., Analysis of Mirnov Oscillations on PDX, Princeton Plasma Physics Lab. Rep. PPPL-1854 (1982).
[8] BEIERSDORFER, P., KAITA, R., GOLDSTON, R.J., Nucl. Fusion **24** (1984) 487.
[9] BUCHENHAUER, D., HWANG, D., GOLDSTON, R., McGUIRE, K., in Heating in Toroidal Plasmas (Proc. 4th Joint Varenna-Grenoble Int. Symp. Rome, 1984), Vol. 1, Int. School of Plasma Physics, Perugia (1984) 111.
[10] GOLDSTON, R.J., McCUNE, D.C., TOWNER, H.H., DAVIS, S.L., HAWRYLUK, R.J., SCHMIDT, G.L., J. Comput. Phys. **43** (1981) 61. McCANN, R.T., GOLDSTON, R.J., McCUNE, D.C., Bull. Am. Phys. Soc. **27** (1982) 971 (description of calculations of beam/beam neutron production).
[11] STRACHAN, J.D., ZANKL, G., Princeton Plasma Physics Lab. Rep. PPPL-TM-353 (1981).
[12] Princeton Plasma Physics Laboratory, Annual Report, October, 1 – September, 30, 1980, Rep. PPPL-Q-38 (1980).

(Manuscript received 24 October 1984
Final manuscript received 18 June 1985)